AFWL-TR-
87-128

EXPERIMENTAL INVESTIGATION OF EMITTANCE GROWTH IN PARTICLE BEAMS USING DIRECTLY HEATED LANTHANUM HEXABORIDE CATHODES

Capt M. McHarg
Lt D. Young

June 1988

Final Report

Approved for public release; distribution unlimited.

AIR FORCE WEAPONS LABORATORY
Air Force Systems Command
Kirtland Air Force Base, NM 87117-6008

UNCLASSIFIED
SECURITY CLASSIFICATION OF THIS PAGE

AD-A196 878

REPORT DOCUMENTATION PAGE

1a REPORT SECURITY CLASSIFICATION Unclassified	1b RESTRICTIVE MARKINGS
2a SECURITY CLASSIFICATION AUTHORITY	3 DISTRIBUTION / AVAILABILITY OF REPORT Approved for public release; distribution unlimited.
2b DECLASSIFICATION / DOWNGRADING SCHEDULE	
4 PERFORMING ORGANIZATION REPORT NUMBER(S) AFWL-TR-87-128	5 MONITORING ORGANIZATION REPORT NUMBER(S)
6a NAME OF PERFORMING ORGANIZATION Air Force Weapons Laboratory 6b OFFICE SYMBOL (If applicable) AWYW	7a NAME OF MONITORING ORGANIZATION
6c. ADDRESS (City, State, and ZIP Code) Kirtland Air Force Base, New Mexico 87117-6008	7b ADDRESS (City, State, and ZIP Code)
8a. NAME OF FUNDING / SPONSORING ORGANIZATION 8b OFFICE SYMBOL (If applicable)	9 PROCUREMENT INSTRUMENT IDENTIFICATION NUMBER
8c. ADDRESS (City, State, and ZIP Code)	10 SOURCE OF FUNDING NUMBERS PROGRAM ELEMENT NO: 61102F; PROJECT NO: 2301; TASK NO: Y1; WORK UNIT ACCESSION NO: 01

11 TITLE (Include Security Classification)
EXPERIMENTAL INVESTIGATION OF EMITTANCE GROWTH IN PARTICLE BEAMS USING DIRECTLY HEATED LANTHANUM HEXABORIDE CATHODES

12 PERSONAL AUTHOR(S)
McHarg M., Capt and Young D., Lt

13a TYPE OF REPORT	13b TIME COVERED	14 DATE OF REPORT (Year, Month, Day)	15 PAGE COUNT
Final	FROM 9/86 TO 8/87	1988, June	34

16 SUPPLEMENTARY NOTATION

17 COSATI CODES			18 SUBJECT TERMS (Continue on reverse if necessary and identify by block number)
FIELD	GROUP	SUB-GROUP	Emittance Growth, Particle Beams, Lanthanum Hexaboride, Cathodes, Nonuniform Radial Intensity Distribution, Electron Gun
20	13		
20	07		

19 ABSTRACT (Continue on reverse if necessary and identify by block number)

This report presents the theory of nonlinear field energy as applied to emittance growth in a space-charge-dominated particle beam. An experiment to validate this theory is described and the experimental apparatus and results are presented. The experimental apparatus is designed around a directly heated lanthanum hexaboride (LaB_6) cathode which yields a variable radial intensity electron distribution. We report the first use of such an electron gun, and its initial operating characteristics, which compare favorably with predicted theory.

20 DISTRIBUTION / AVAILABILITY OF ABSTRACT ☒ UNCLASSIFIED/UNLIMITED ☐ SAME AS RPT ☐ DTIC USERS	21 ABSTRACT SECURITY CLASSIFICATION Unclassified
22a NAME OF RESPONSIBLE INDIVIDUAL Dr Yolanda D. Jones	22b TELEPHONE (Include Area Code) (505) 844-1786 22c OFFICE SYMBOL AWYW

DD FORM 1473, 84 MAR 83 APR edition may be used until exhausted
All other editions are obsolete

SECURITY CLASSIFICATION OF THIS PAGE
UNCLASSIFIED

CONTENTS

FIGURES

INTRODUCTION

Understanding the phenomena of emittance growth in space-charge-dominated particle beams is of importance to any application that requires a small final emittance. Many researchers have looked at the process of emittance growth under these conditions (Refs. 1-6). Wangler, et al., (Ref. 1) uses the idea of nonlinear field energy to describe emittance growth. In brief, a beam with a nonuniform radial intensity distribution has a potential energy associated with this distribution. As the beam propagates through the magnetic optic, this potential energy is turned into transverse kinetic energy and manifests itself as emittance growth.

This report briefly reviews this theory. An experiment to check the validity of the theory is described, and some of the details associated with the experiment are enumerated. The third section describes the apparatus used in this experiment, which includes an electron gun that yields beams with a variable radial intensity distribution. The gun uses a directly heated lanthanum hexaboride (LaB_6) cathode to produce the variable intensity beam. The characteristics of this electron gun are given in the fourth section.

THEORY

Studies by Wangler, et al., on the relationship between nonuniform radial distributions and emittance growth in a space-charge-dominated transport system, have recently been published (Ref 1). A nonlinear differential equation was shown to govern the emittance as a function of the position along the transport line. This differential equation was also derived by Lapostolle (Refs. 2 and 3) and by Lee, Yu, and Barletta (Ref 4) for a beam with no external focusing.

$$\frac{d\epsilon^2}{dz} = - \frac{x^2 K}{2} \frac{d}{dz}\left(\frac{U}{W_0}\right) \tag{1}$$

where x (twice the RMS beam radius is defined as $x = 2\sqrt{\overline{x^2}}$) is interpreted as the total beam radius of an equivalent uniform beam, and k is the generalized perveance given by

$$K = \frac{qI}{2\pi\epsilon_0 m v^3 \gamma^3} \tag{2}$$

and

$$U = W - W_U \tag{3}$$

Here W is the field energy given by

$$W = \pi\epsilon_0 \int^{\infty} r\, E_r^2\, dr \tag{4}$$

and the field energy of a uniform beam, W_U, is given by

$$W_U = W_0\left(1 + 4 \ln \frac{b}{x}\right), \quad b \geq x \tag{5}$$

where

$$W_0 = \frac{(qN)^2}{16\pi\epsilon_0} \tag{6}$$

N is the number of particles per unit length, and b is the radius larger than x that defines a volume over which the real beam is averaged. Equation 1 is integrated and assumes an RMS-matched beam with constant x. The resulting equation relates RMS emittance and the term U/w_0, called the nonlinear field energy.

$$\frac{\varepsilon}{\varepsilon_i} = \left[1 - \frac{(U - U_i)}{2w_0}\left(\frac{\omega_0^2}{\omega_i^2} - 1\right)\right]^{1/2} \tag{7}$$

where ω_0 is the zero current betatron frequency, ω_i is the initial betatron frequency for an equivalent beam including space charge, and ε_i, U_i are the initial emittance and nonlinear field energy, respectively.

Quoting Wangler, et al., "We find that U/w_0 is zero for a uniform charge distribution and is positive both for peaked and hollow distributions, increasing as the distribution becomes more nonuniform. Furthermore, U/w_0 is independent of both beam current and RMS beam size, and is only a function of the shape of the distribution" (Ref. 1). Thus, the analytic result of this equation is clear; if the beam distribution is flat, then zero emittance growth will occur.

Excellent agreement between these analytic predictions and computer calculations have been obtained to support this theory (Ref. 1). The final value for the nonlinear field energy must be known before Eq. 7 can be used to predict emittance growth in real systems. In the computer simulations, the nonlinear field energy was observed to change as a function of the distance the particles traveled along the magnetic optic.

To enable an analytic estimation of the final emittance growth, Wangler, et al., made the approximation that the final nonlinear field energy would evolve to a steady-state value of zero. This estimation will be quite accurate for a space-charge-dominated beam, where the emittance growth is largest. For an emittance-limited case, this approximation will provide an upper bound for the emittance growth observed. Equation 8 is an approximation to Eq. 7.

$$\frac{\varepsilon_f}{\varepsilon_i} = \left[1 - \frac{U_i}{2w_o} \left(\frac{\omega_o^2}{\omega_i^2} - 1 \right) \right]^{1/2} \tag{8}$$

Figure 1 shows a graph from Ref. 1 that compares Eq. 8 to the computer simulation discussed previously. As can be seen, there is good agreement between the two. This comparison is made after 100 plasma oscillations, where the length, λ_p, is defined as

$$\lambda_p = \left(\frac{2\pi^2 x^2}{k\gamma^2} \right)^{1/2} = \left(\frac{4\pi^3 x^2 \varepsilon_o m v^3 \gamma}{qI} \right)^{1/2} \tag{9}$$

and is the distance the beam travels during one plasma period.

Reiser (Ref. 5) shows that the initial betatron tune ratio, ω_i/ω_o, is given by

$$\frac{\omega_i}{\omega_o} = \frac{\varepsilon}{\alpha} = \frac{\varepsilon 2 m_o c \beta \gamma}{r^2 q B_z}, \quad \alpha = r^2 \sqrt{k_s} \tag{10}$$

where r is the matched beam radius. This radius is given by solving the envelope equation with the second-order differential term set equal to zero (Ref. 5) resulting in Eq. 11,

$$k_s r^4 - K r^2 - \varepsilon^2 = 0 \tag{11}$$

where k_s is the external focusing force of the solenoid (Ref. 5).

$$k_s = \left(\frac{q B_z}{2 m_o c \beta \gamma} \right)^2 \tag{12}$$

Inserting Eq. 10 into Eq. 8, and using the field energy constant for a Gaussian beam given by Wangler, et al., (Ref. 1), we obtain

$$\frac{\varepsilon_f}{\varepsilon_i} = \left[1 + \frac{0.154}{2} \left(\left[\frac{r^2 q B_z}{\varepsilon 2 m_o c \beta \gamma} \right]^2 - 1 \right) \right]^{1/2} \tag{13}$$

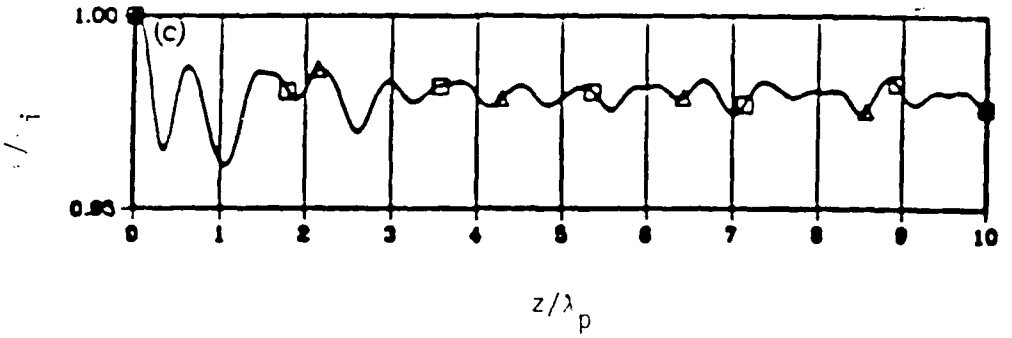

(a) Flat distribution.

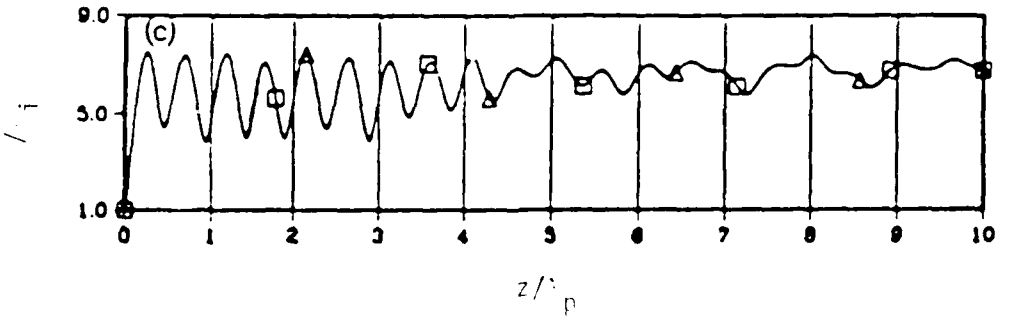

(b) Peaked distribution.

Figure 1. Analytical prediction of emittance growth.

Equation 9 is then solved to yield the energy of the beam required to obtain a given plasma period.

$$E = \frac{m}{2}\left(\frac{\gamma_p q I}{4\pi^3 x^2 \varepsilon_0 m}\right)^{2/3} \tag{14}$$

where $E = mv^3/2$.

Equations 14, 13 (when solved for B_z), and 11 are coupled equations which yield the experimental conditions necessary to check the theory.

To aid solving these three nonlinear equations, rewrite them in terms of the unknowns B_z, E, R, and constants α, β_1, β_2, β_3, γ_1, γ_2. Assume that x in Eq. 14 is equal to R in Eq. 11.

$$E - \frac{\alpha}{R^{4/3}} = 0 \tag{15}$$

$$\frac{\beta_1 B_z^2 R^4}{E} - \frac{\beta_2 R^2}{E^{3/2}} - \beta_3 = 0 \tag{16}$$

$$\gamma_1 - \frac{\gamma_2 R^4 B_z^2}{E} = 0 \tag{17}$$

where

$$\alpha = \frac{m_0}{2}\left(\frac{\lambda_p^2 q I}{4\pi^3 \varepsilon_0 m}\right)^{2/3}$$

$$\beta_1 = \frac{q^2}{8m_0}$$

$$\beta_2 = \frac{qI}{2\pi\varepsilon_0 m_0 \left(\frac{2}{m_0}\right)^{3/2}}$$

$$\beta_3 = \varepsilon^2$$

$$\gamma_1 = \left[\left(\frac{\varepsilon_f}{\varepsilon_i}\right)^2 - 1\right]\frac{2w_0}{U_0} + 1 \text{ , and}$$

$$\gamma_2 = \frac{q^2}{8\varepsilon^2 m_0}$$

Solving Eq. 17 for $R^4B_z^2/E$ and substituting into Eq. 16, we obtain

$$\frac{\beta_1\gamma_1}{\gamma_2} - \frac{\beta_2 R^2}{E^{3/2}} - \beta_3 = 0 \tag{18}$$

Solving Eq. 15 for $E^{3/2}$ and substituting into Eq. 18, we obtain

$$\frac{\beta_1\gamma_1}{\gamma_2} - \frac{\beta_2 R^4}{\alpha^{3/2}} - \beta_3 = 0 \tag{19}$$

We now solve directly for E, R, and B_z respectively.

$$R = \left[\frac{\alpha^{3/2}}{\beta_2}\left(\frac{\beta_1\gamma_1}{\gamma_2} - \beta_3\right)\right]^{1/4} \tag{20}$$

$$E = \frac{\alpha}{R^{4/3}} \tag{21}$$

$$B_z = \left(\frac{\gamma_1 E}{\gamma_2 R^4}\right)^{1/2} \tag{22}$$

To evaluate the constants, we need to know λ_D, I, ε, $\varepsilon_f/\varepsilon_i$, and w_0/U_0. The plasma period is related to the length of the solenoid. Since the magnetic field needs to be many plasma periods long, the plasma period needs to be fairly short. The current and the emittance are determined by the electron gun design. The last two parameters are determined by the beam profile and the amount of emittance growth desired. Table 1 shows E, R, and B_z for the

parameters shown. Here we have assumed I = 10 mA, λ_p = 20 cm and ϵ = 2.5510^{-3} mrad (estimated from acceptance of electron gun).

Table 1. Calculated parameters.

$\frac{\epsilon_f}{\epsilon_i}$	R(cm)	E(eV)	B_z(Gauss)
1*	-	-	-
2	2.7	57	11.5
3	3.4	42	9.7
4	4.0	34	8.7
5	4.6	29	8.1
6	4.9	25	7.6
7	5.3	23	7.2
8	5.7	21	6.8
9	6.0	19.3	6.4
10	6.4	18	6.4

*For ϵ_f/ϵ_i = 1, no solution was obtainable because β_3 was greater than $\beta_1\gamma_1/\gamma^2$ for the parameters chosen.

Note that most of the emittance growth is seen in the first plasma period (Ref. 6). Thus there are two ways to perform an experiment to check the theory. The first experiment would use a solenoidal field of many plasma periods in length that enabled the final beam energy to relax to zero. The energy, magnetic field and radius of the beam would be varied as shown in Table 1 to produce the emittance growth predicted. The second experiment would use a solenoidal field of one plasma period or less with a fixed tune depression. The emittance growth seen could then be compared with the results predicted in Eq. 8 as a function of z/λ_p.

For either of the experiments, a beam with a variable intensity distribution is needed. This will allow the emittance growth for a peaked and flat beam to

be checked against the theory. One electron gun should be used to produce both profiles to ensure that emittance growth caused by factors other than space charge is present in the same amount for each experiment. The next section details the experimental apparatus used to achieve a peaked and flat profile beam in the same electron gun.

EXPERIMENTAL APPARATUS

The experimental apparatus consists of an electron gun with variable intensity profile, a solenoid magnet, and an emittance measurement device. The entire experiment is run at a pressure of 10^{-6} torr in a vacuum tank evacuated by cryogenic pumps.

The electron gun with a variable intensity profile is the heart of the experimental device. To achieve a variable intensity beam, a directly-heated lanthanum hexaboride (LaB_6) cathode was used. The cathode is a thermionic emitter, so the temperature profile across the cathode determines the emission profile of the electrons. Thus the profile is changed by changing the temperature profile on the cathode.

The cathode is heated in a coaxial manner with the current flowing through a center rod, across the cathode face, and returning through an outer graphite connector attached to the outside ring of the cathode. The coaxial design results in a free-field emission region in front of the cathode. Figure 2 shows the cathode assembly in a disassembled picture. The graphite center rod and outer "fingers" are clearly visible along with the LaB_6 cathode. The entire assembly is cooled via an external cooling jacket.

Graphite is used in the cathode assembly since degradation of the LaB_6 cathode occurs if it comes in contact with most metals (Ref. 7). The outer graphite connector is a cylindrical tube with pipe threads cut into one end and 24 fingers cut into the other. The ends of the fingers are beveled inward and make contact with the edge of the cathode. These fingers are made by cutting 2.54-cm-long slots, 0.064 cm wide, into the graphite connector. The inside diameters of the fingers are radiused at the bottom of the slot to reduce breakage of the fingers under thermal and mechanical stress.

The graphite inner connector determines the temperature profile across the face of the cathode. Two different inner connectors are used to produce the two differing temperature profiles. For the flat distribution, the inner connector is a threaded hollow tube about 2.54-cm-long containing a disk

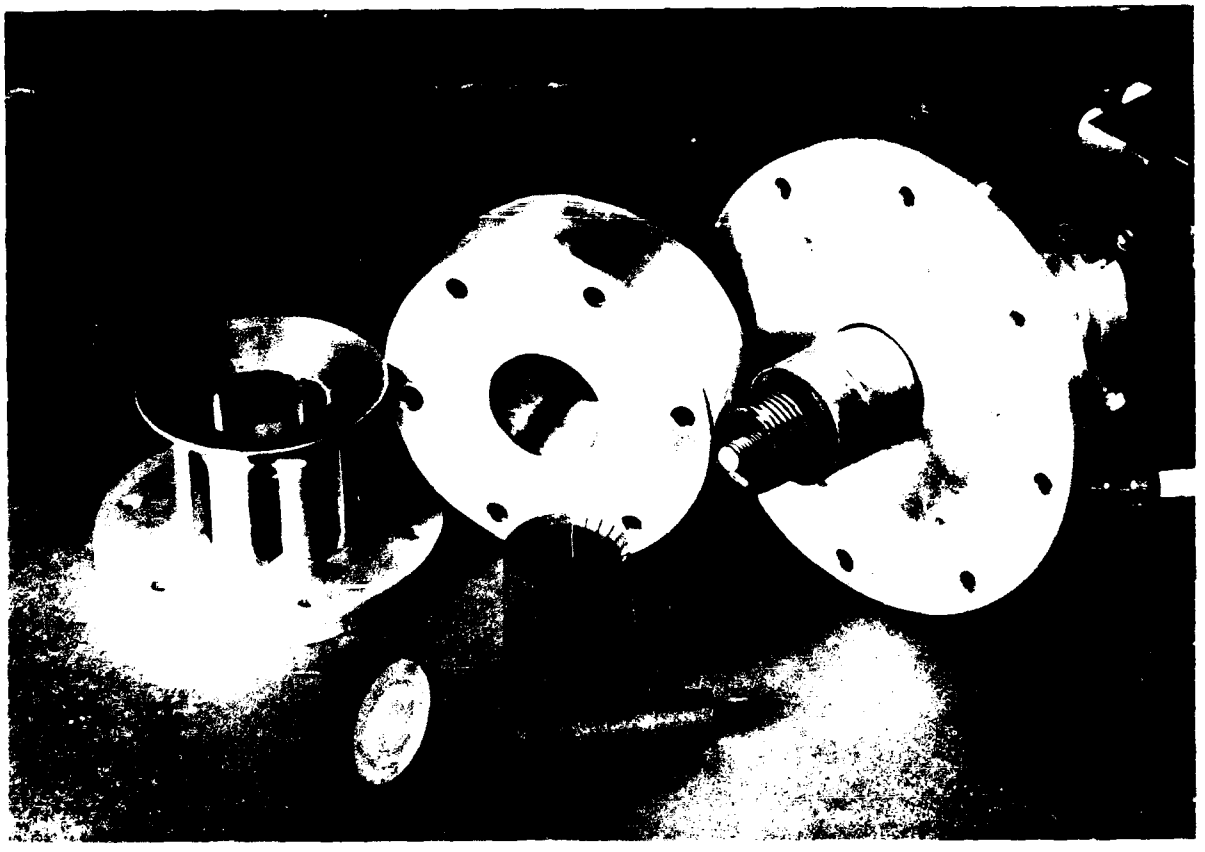

Figure 2. Picture of disassembled cathode.

0.3175 cm thick. This disk makes contact between the copper rod and the LaB_6 cathode. The distribution can be fine tuned by adjusting the tension in the fingers of the outer connector.

For a peaked distribution, the inner connector is a solid graphite rod with threads cut into both ends. The threaded end which makes contact with the cathode is tapered. The angle of the taper affects the peaked distribution; generally a larger taper angle increases the center temperature of the cathode.

In both cases, the cathode is pushed against the outer connector, resulting in the fingers spreading outward. The tension on the cathode is directly related to the distance the fingers are spread. Best operating conditions were obtained for the cathode when the fingers were spread from the unstressed diameter of 2.54 cm to the stressed diameter of 2.576 cm.

The electron gun was designed to give a 3000-V, 30-mA beam. A Pierce cathode geometry was chosen for ease of design and a focused beam (Ref. 8). The anode is a flat plate with an aperture of 1.91 cm. The cathode/cooling jacket assembly is held at the same potential as the Pierce cathode. The anode is connected to system ground, and the cathode assembly floated to the final operating voltage. The anode/cathode gap is variable, and was optimized at 3.81 cm for the beam parameters desired. Figure 3 shows the electron gun assembled with the Pierce cathode in place.

The cathode was heated with a pair of Advance A1500 5-V, 300-A power supplies. The power supplies were run in parallel, yielding 5 V, 600 A. The accelerating potential power supply was changed several times due to limited beam current available from the supply. The final supply chosen was a 3-kV, 30-mA Fluke high-voltage supply.

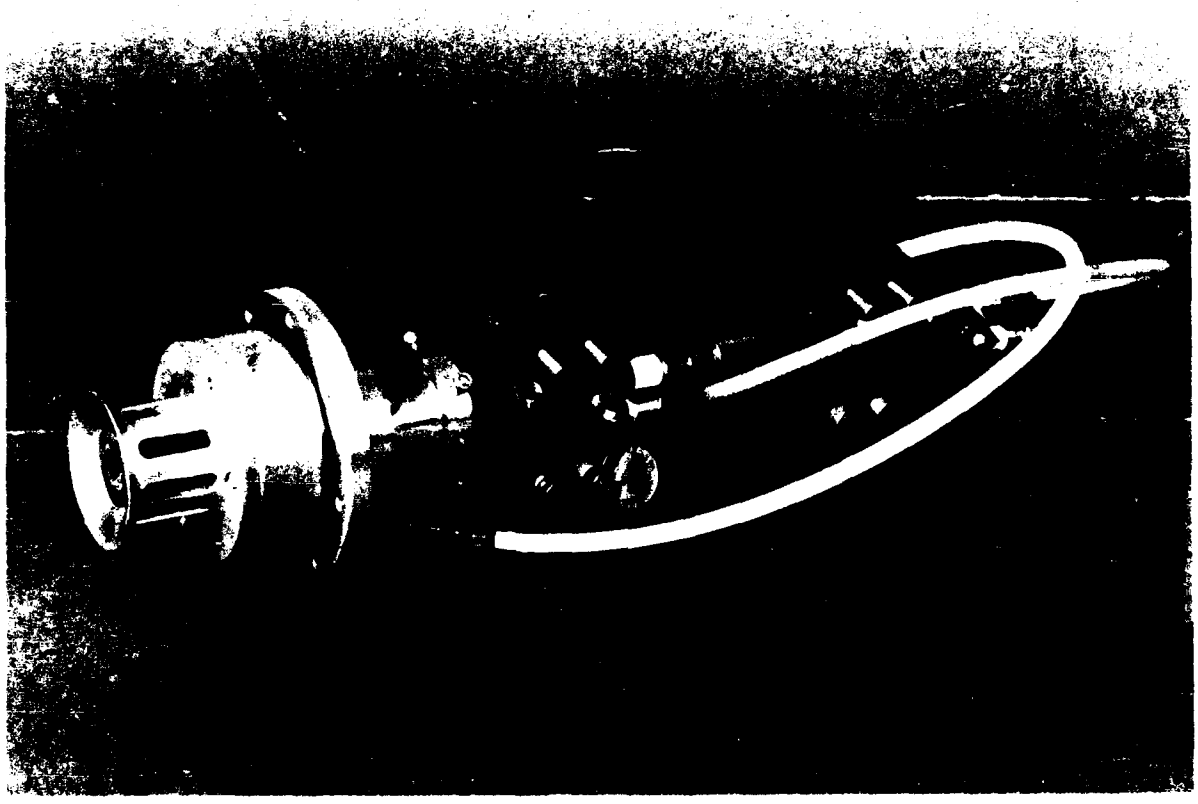

Figure 3. Picture of assembled electron gun.

EXPERIMENTAL RESULTS

The experimental results are presented in three categories. The first category details the temperature of the cathode as a function of heater power delivered to the cathode. The second details the beam current as a function of various parameters. The last details the electrical properties of the cathode as a function of temperature.

Two diagnostic devices were used to find the cathode temperature. The first was an optical pyrometer, which was used to find center temperatures and rough temperature profiles across the face of the cathode. The second was an Inframetrics infrared (IR) imaging camera. This camera gave detailed temperature profiles of the cathode. The camera operates in the 5- to 15-μm range and requires the use of a zinc selenide window for IR transmission. Since the optical pyrometer required a Plexiglas window, use of the two diagnostics at the same time was quite difficult.

The Inframetrics camera was sensitive to changes in the zinc selenide window. Dirt particles, oil, and water vapor on the surface of the window appeared as hot and cold spots on the cathode. These problems were minimized by increased care of the window. The camera was also sensitive to emissivity changes in the LaB_6 cathode itself.

During the experiment, the LaB_6 cathode reacted with residual oxygen in the system and created deposits of $LaBO_3$ on the surface of the cathode. This changed the emissivity of the surface, and finally required termination of use of th.. IR camera. The optical pyrometer was less sensitive to emissivity changes, and was used throughout the experiment to obtain temperature measurements.

Figure 4 shows the surface of the cathode after the $LaBO_3$ deposits had become apparent. The composition of the deposit was determined using X-ray diffraction techniques. The cathode was cleaned using hydrochloric acid. Figure 5 shows the cathode after cleaning. The obvious deposits are gone, with the X-ray diffraction data showing no signs of $LaBO_3$. The deposits occurred at pressures above 10^{-6} torr.

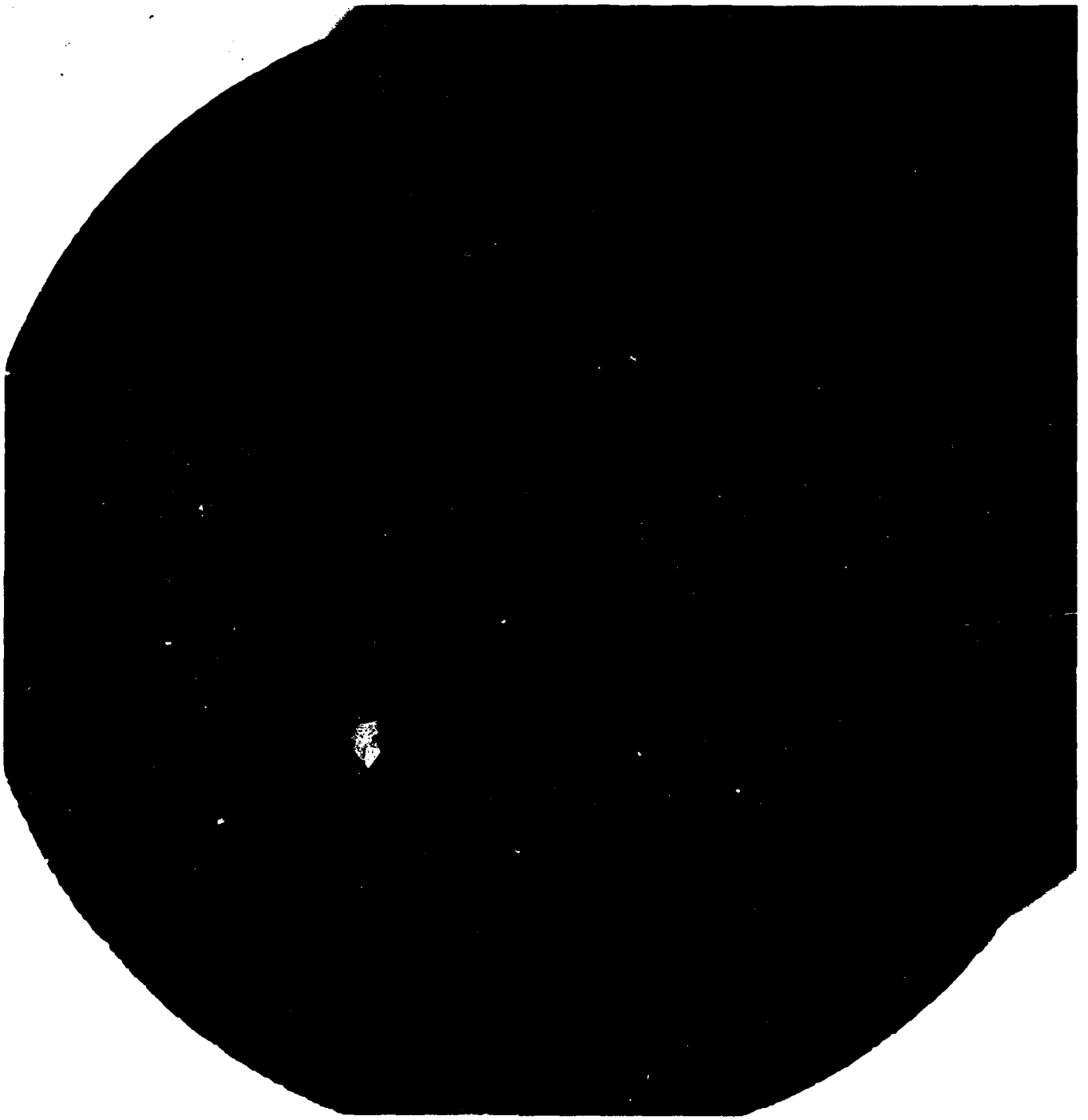

Figure 4. LaB_6 cathode close-up before cleaning.

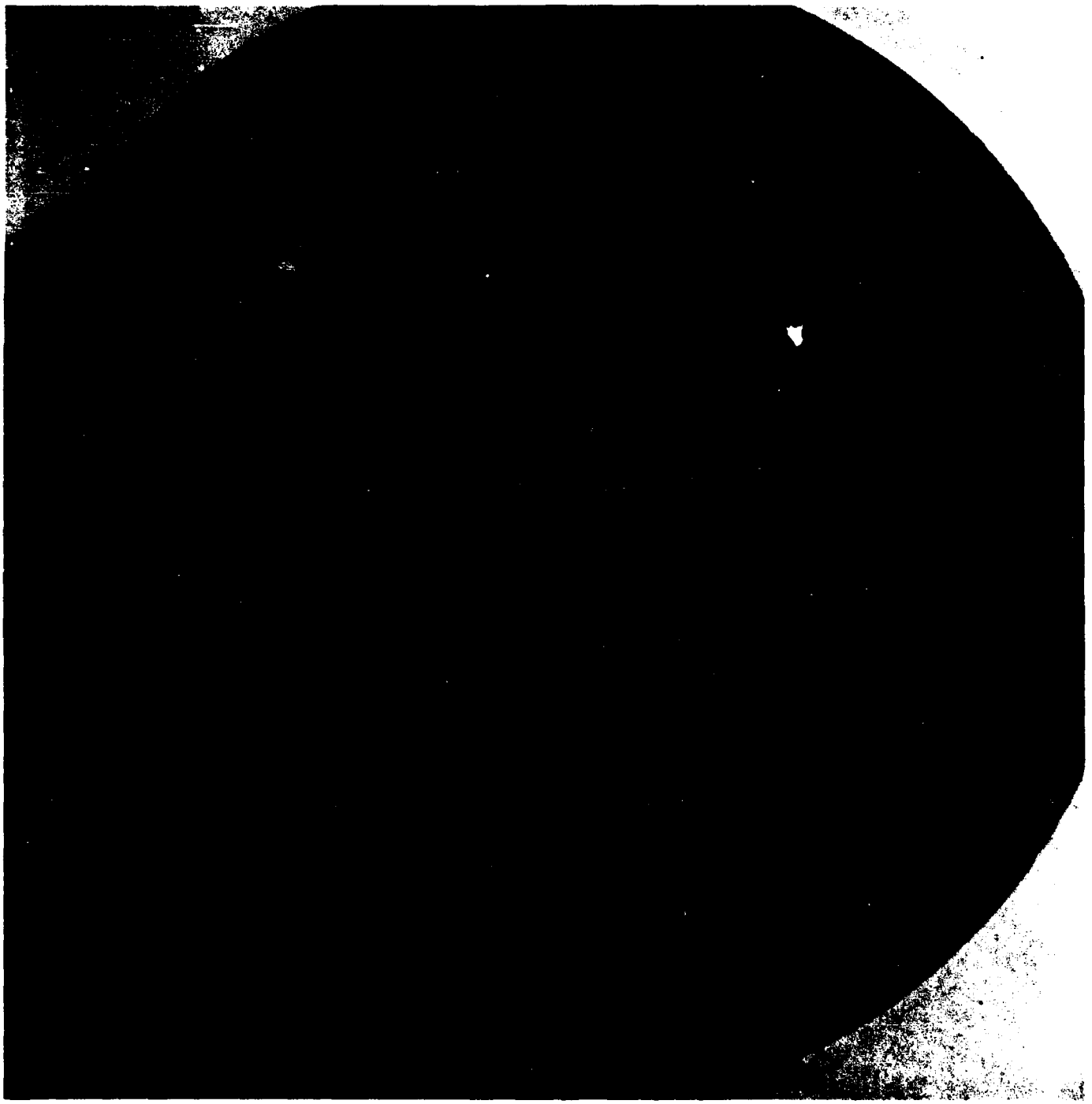

Figure 5. LaB_6 cathode close-up after cleaning.

Figures 6 and 7 show the center temperature of the cathode as a function of heater power for the peaked and flat distribution. Data from both the pyrometer and the IR camera are presented. In both cases there is roughly a 200°C difference between the two measurement techniques at similar powers. The difference between the two measurement techniques is still unresolved. This difference may be due to sensitivity of the camera to emissivity changes, or to changes in the electrical characteristics of the cathode. The figure is a compilation of different experimental runs, and some changes were observed in the resistance of the cathode as a function of power during different runs.

The optical pyrometer data were chosen as the reportable data because they are less sensitive to changes in emissivity. The IR camera is used to show the relative shape of the temperature profile as seen in Fig. 8. Here the peaked and flat profiles are seen in the line scan mode of the IR camera. The flat profile is uniform to within 1 percent. The center of the peaked distribution is 25°C hotter than the edge of the distribution. This difference can be increased if desired by changing the taper angle on the center conductor and the tension of the outer conductor.

The beam current obtained for the temperature distributions is shown in Fig. 9. The current was measured using a graphite Faraday cup biased to 300 V to reduce secondary electron emission effects on the current measurement. The beam current was power-supply and space-charge limited. In no case was the emission limit reached.

Figure 10 shows curves for different accelerating potentials as a function of beam power. The two curves are for 500 and 1000 V. The effects of the space charge limit are clearly seen in these two curves. The data show that the current approaches the limit predicted by theory (Ref. 9).

In all cases, after the cathode had been let up to atmosphere the electron current was greatly reduced. This agrees with other studies of LaB_6 emission (Ref. 10). Figure 11 shows the increase in current as a function of time at a power of 830 to 940 W. As can be seen, the current reaches a steady state after an elapsed time of 10-15 min.

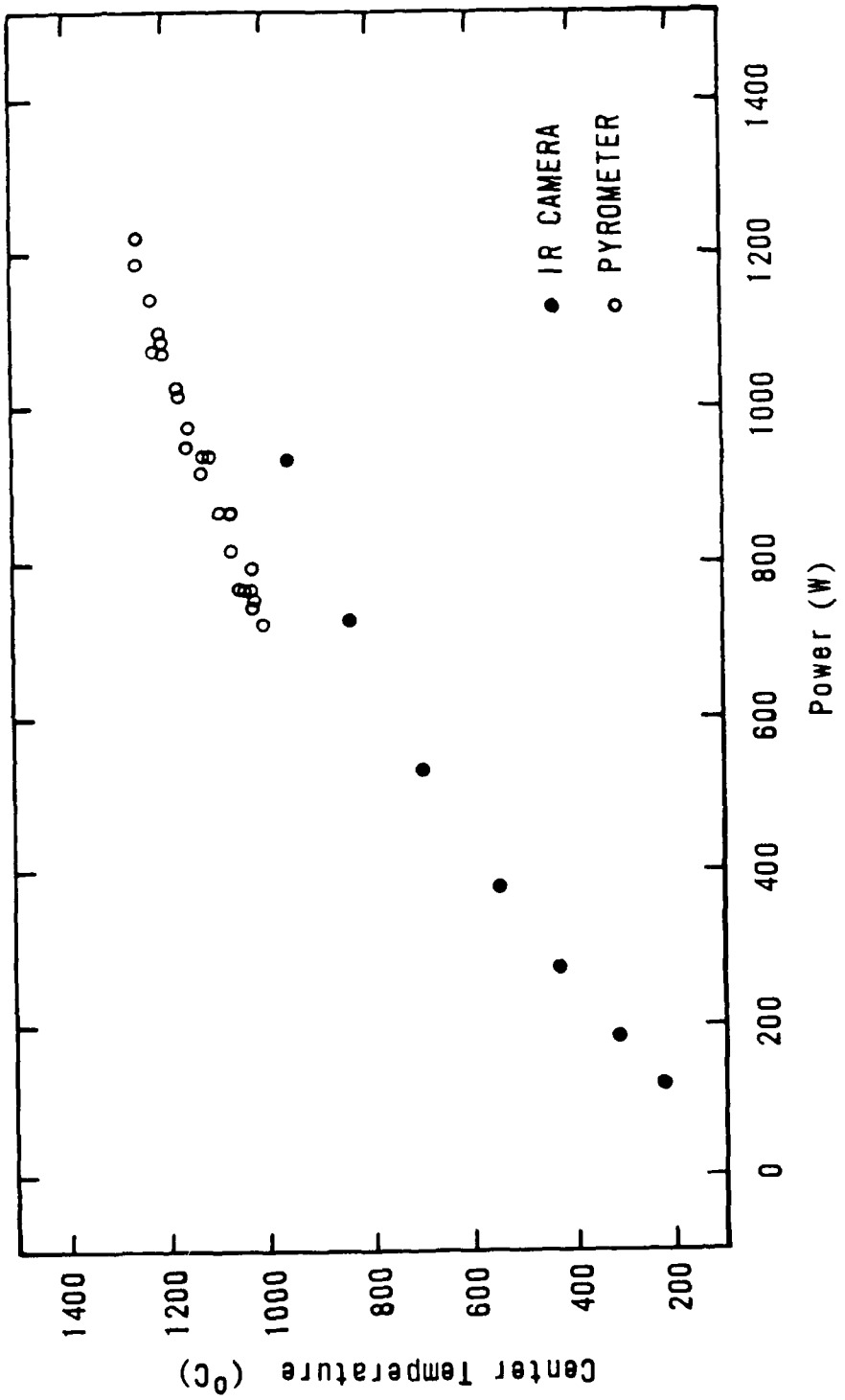

Figure 6. Center temperature versus power for pyrometer and infrared camera, peaked distribution.

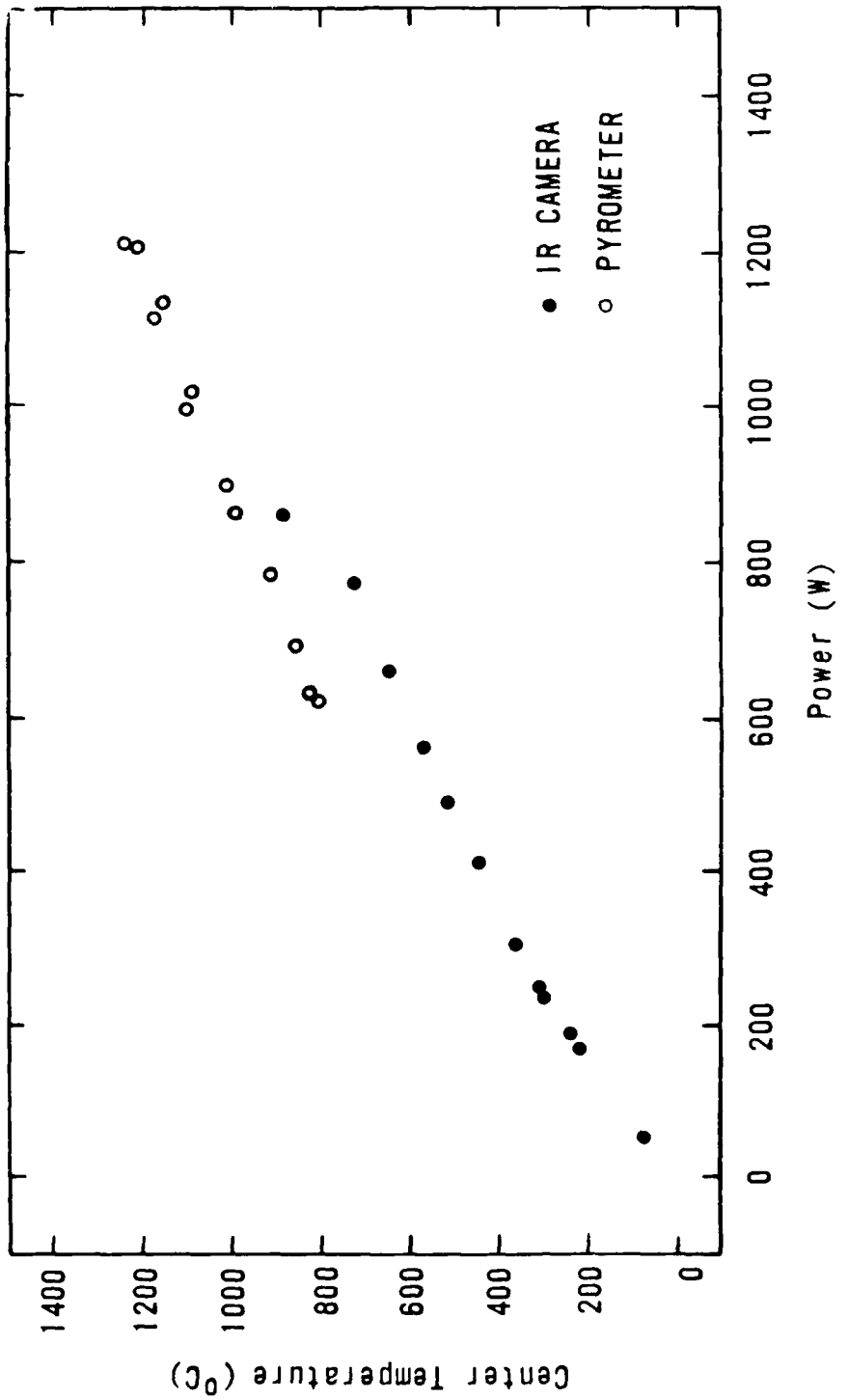

Figure 7. Center temperature versus power for pyrometer and infrared camera, flat distribution.

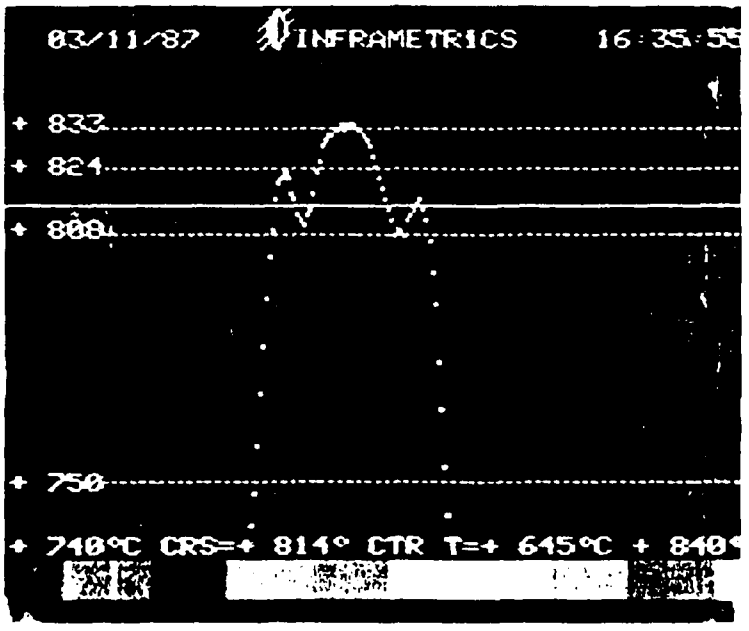

(a) Peaked.

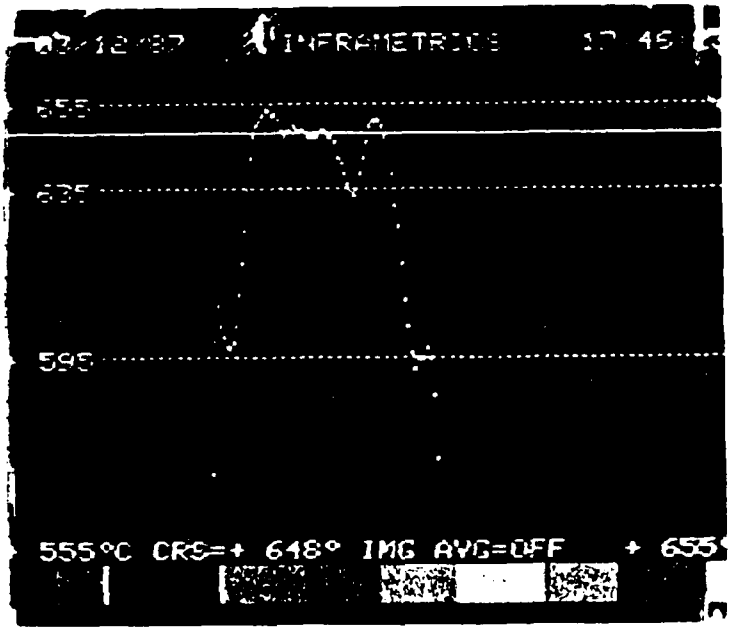

(b) Flat.

Figure 8. Line scan of peaked and flat distribution.

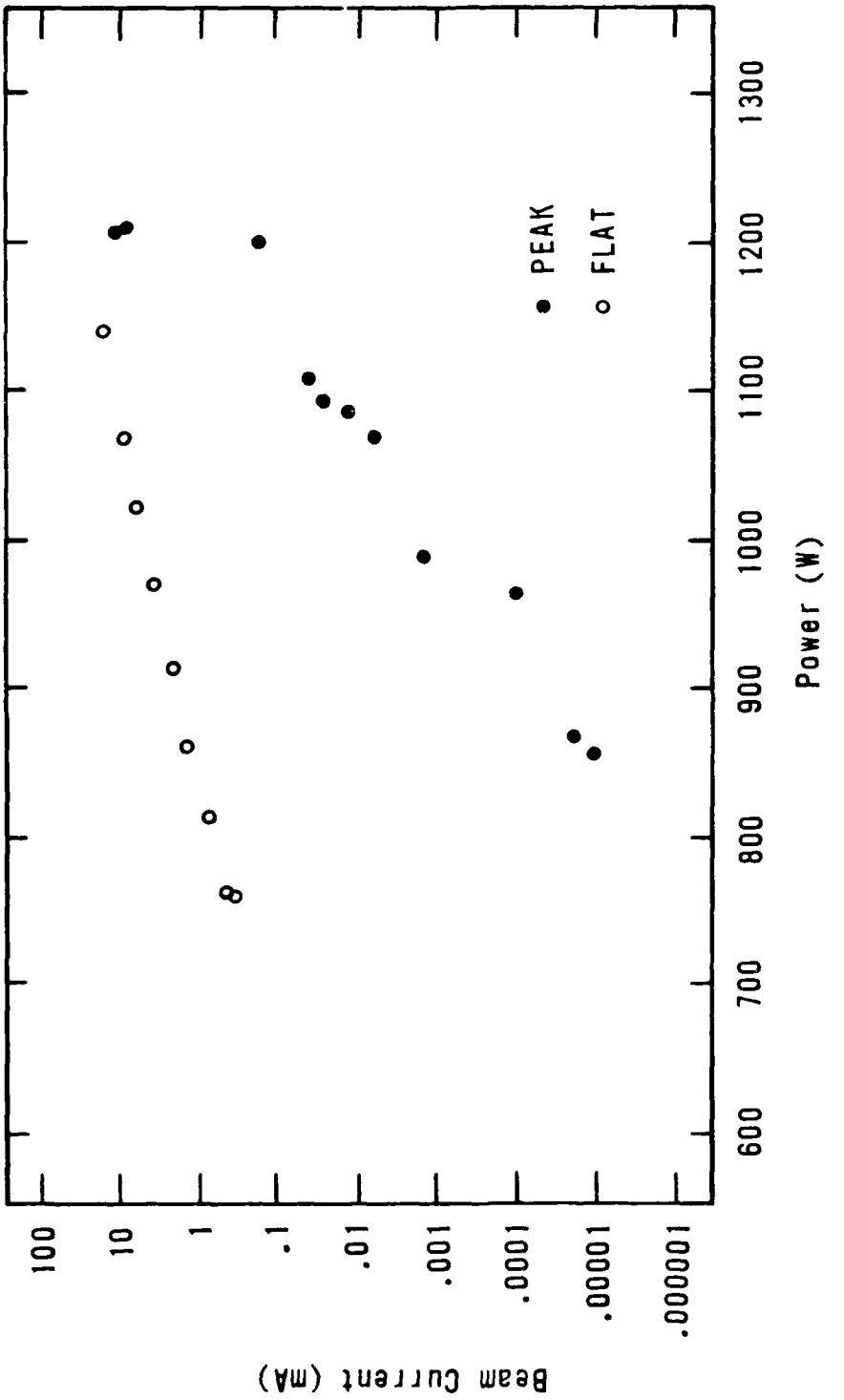

Figure 9. Beam current versus power, peaked and flat.

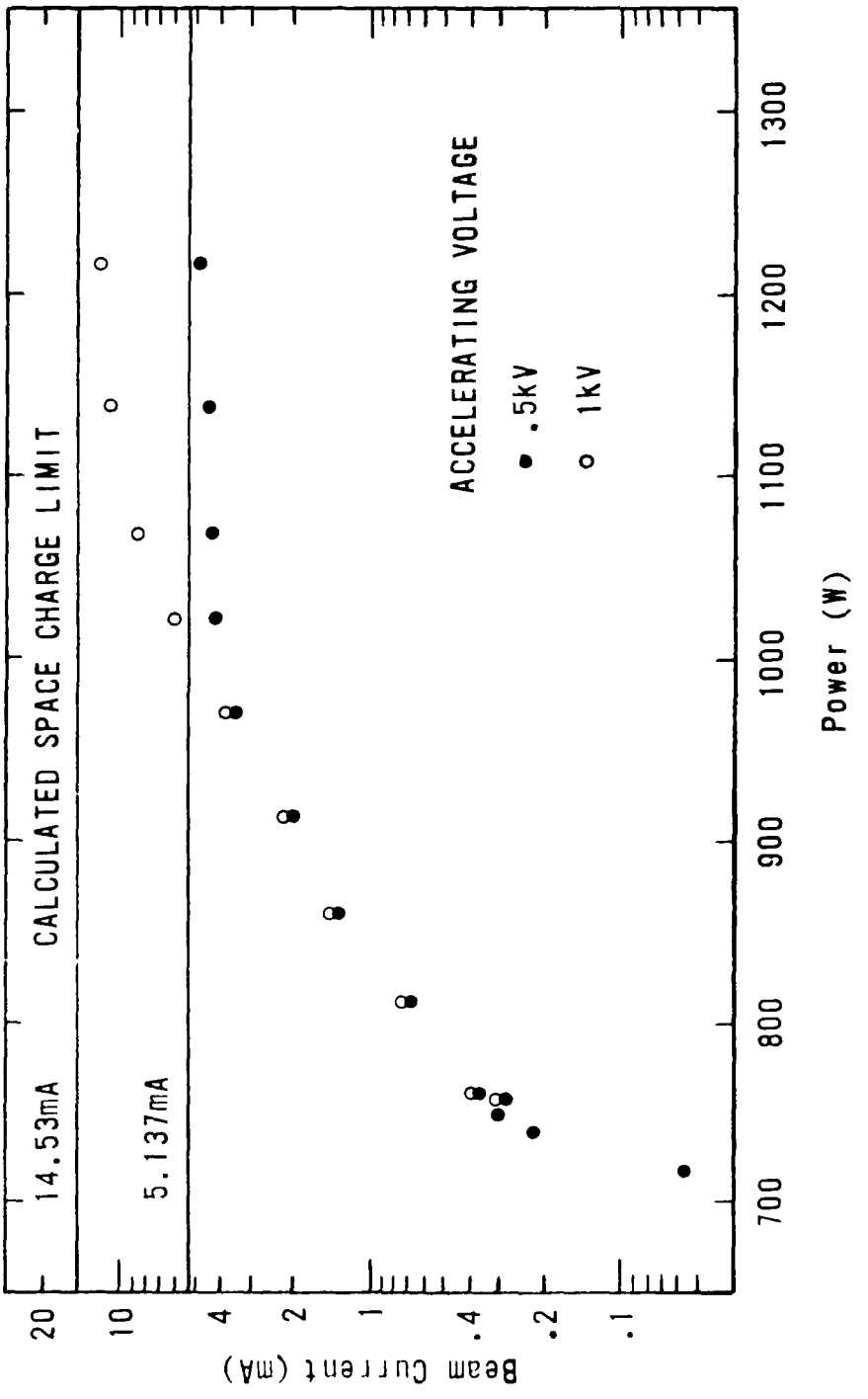

Figure 10. Beam current versus power showing space charge.

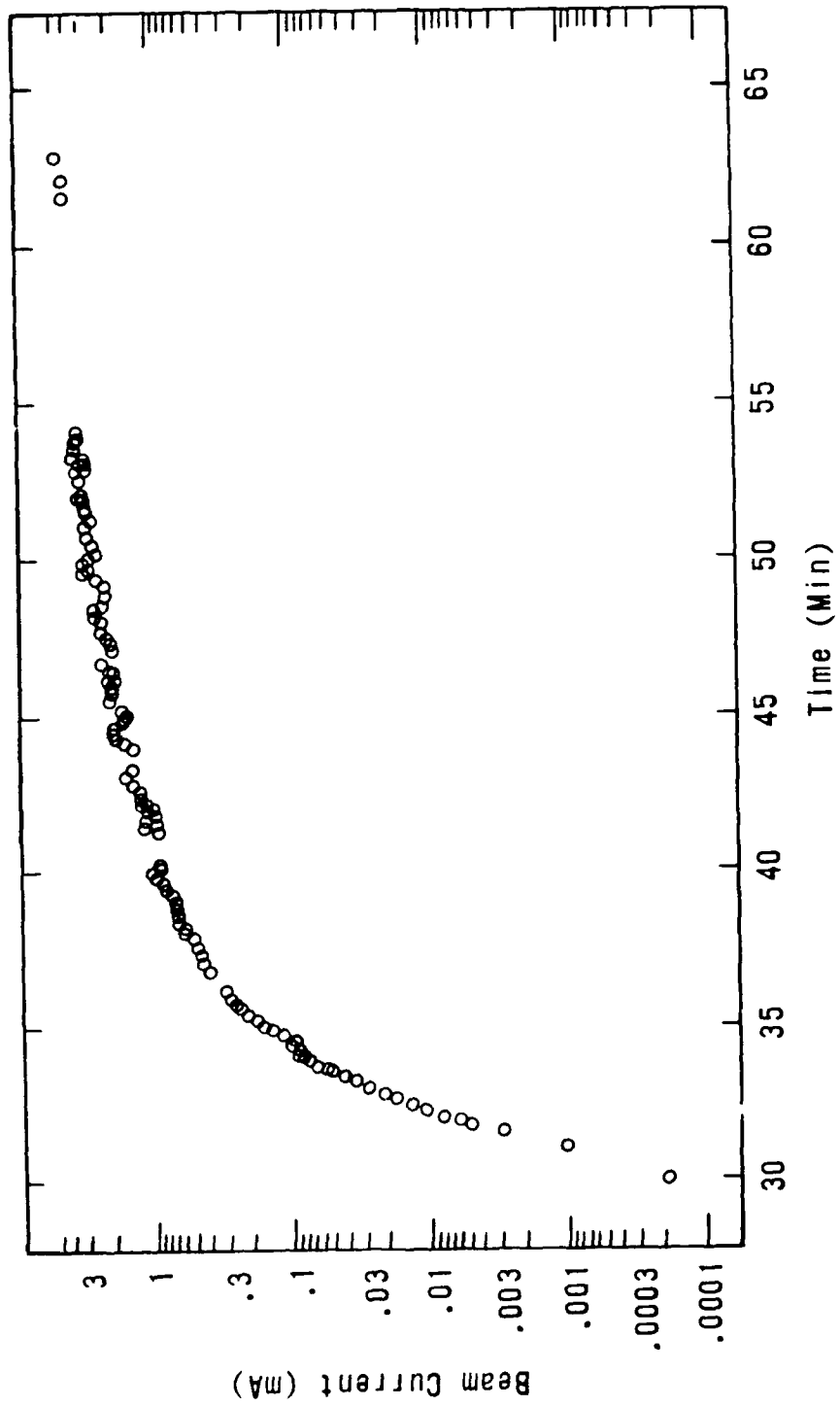

Figure 11. Poisoning bakeout.

Electrical characteristics of the cathode assembly are seen as a function of heater power in Fig. 12. The flat distribution has a lower overall resistance. The peaked distribution required lower powers to reach similar temperatures and currents when compared to the flat distribution. The difference in resistance is due to the length of the inner graphite connector.

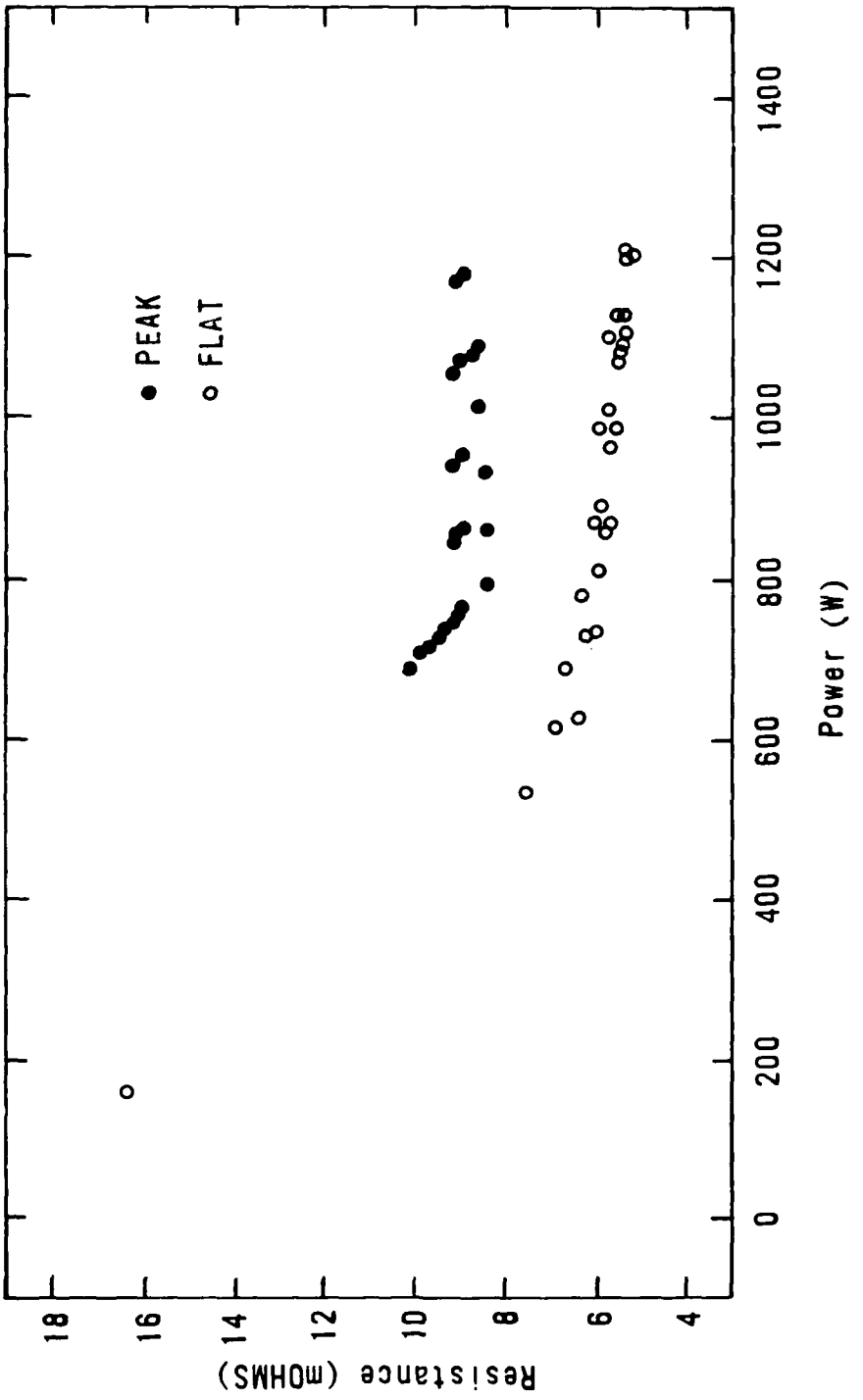

Figure 12. LaB_6 resistance versus power.

CONCLUSIONS

The theory and partial experimental results for measuring the emittance growth due to nonlinear field energy have been presented. An electron beam with variable intensity distribution based on a directly heated LaB_6 cathode has been assembled and tested. Beam parameters necessary for the experiment have been produced on a repeatable basis.

Emittance measurements on the electron beam have not yet been performed. These measurements, plus the construction of a solenoid with parameters shown in Table 1, are the remaining tasks necessary to complete the experiment.

A theoretical understanding of emittance growth due to nonlinear field energy would greatly assist in the design and manufacture of high-quality, low-divergence magnetic optics for many applications. Since a theory requires verification by experiment, further testing is recommended.

REFERENCES

1. Wangler, T. P., Crandall, K. R., Mills, R. S. and Reiser, M., "Relation Between Field Energy and RMS Emittance In Intense Particle Beams," IEEE Trans. Nucl. Sci., Vol. 32, No. 5, p. 2196, 1985.

2. Lapostolle, P. M., "Energy Relationships in Continuous Beams," Los Alamos National Laboratory translation LA-TR-80-8, or CERN-ISR-DI/71-6, 1971.

3. Lapostolle, P. M, "Possible Emittance Increase Through Filamentation Due to Space Charge in Continuous Beams," IEEE, Trans. Nucl. Sci., Vol. 18, No. 3, p. 1101, 1971.

4. Lee, E. P, Yu, S. S., and Barletta, W. A., "Phase Space Distortion of a Heavy Ion Beam Propagation Through A Vacuum Reactor Vessel," Nuclear Fusion, Vol. 21, p. 961, 1981.

5. Reiser, M., "Periodic Focussing of Intense Beams," Particle Accelerators, Vol. 8, pp. 167-182, 1978.

6. Anderson, O. A., "Some Mechanisms and Time Scales For Emittance Growth," AIP Conf Proc., Vol. 152, pp. 253-263, 1986.

7. Goebel, D. M., Hirooka, Y., and Sketchley, T. A., "Large Area Lanthanum Hexaboride Electron Emitter," Review of Scientific Instruments, Vol. 56, No. 9, September 1985.

8. Pierce, J. R., Theory and Design of Electron Beams, pp. 176-178, Van Nostrand Reinhold Co., New York, N. Y., 1954.

9. Brook, D. L., "NRL Plasma Formulary," Naval Branch Laboratory, Washington D.C., 1980.

10. Gallagher, H. E., "Poisoning of LaB_6 Cathodes," Journal of Applied Physics, Vol. 40, January 1969.

★ US GPO